PHYSICSAccess Research Paper
ISSN Online: 2756-3898, ISSN Print: 2714-500X https://doi.org/10.47514/phyaccess.2023.3.1.001

Effect of Single Atom Doping on Structural, Electronic and Magnetic Properties of Hexagonal Silicon Carbide (4H-SiC) for Spintronic Application: A first principle study

Yakubu A Tanko[1], Oyedare T Maha[1], Alhassan Shuaibu[1] and Peter Olusola[2]

[1] Department of Physics, Kaduna State University, Kaduna, PMB 2339, Kaduna State, Nigeria
[2] Department of Science Laboratory Technology, Federal Polytechnic Ede, Osun State, Nigeria

Corresponding E-mail: alhassan.shuaibu@kasu.edu.ng

Received 02-12-2022
Accepted for publication 09-02-2023
Published 10-02-2023

Abstract

In this paper, the structural geometry, electronic and magnetic properties of single magnesium (Mg) and vanadium (V) atoms doped 4H-SiC system were investigated. For the structural geometry of each sample, the energy substitution, as well as bond length, were calculated; results obtained indicate that the bond length of Silicon-Magnesium (Si-Mg) and Silicon-Vanadium (Si-V) was 1.90 Å and 2.02 Å respectively, greater than that of silicon-carbon (Si-C) 1.89 Å in pure SiC. This result indicates that the bond length increases due to the introduction of dopants with greater radii than that of Si. It also shows that both Mg and V doping changes the structure from non-magnetic ordering to magnetic in nature. The band structure result for both undoped and doped shows the presence of valence band maximum (VBM) and conduction band minimum (CBM) around different symmetry points which indicate an indirect band gap nature. The calculated band gap of pure 4H SiC is found to be ~ 2.21 eV, which is at a wide band gap material range, but with the introduction of Mg and V dopants, the band gap reduced significantly to ~0.4 eV and ~0.45 eV respectively. The density of state (DOS) and projected density of state (PDOS) show the contributions of the various states in both the VBM and CBM; after doping the Fermi energy is shifted towards higher energy and enters into the conduction band, exhibiting spin polarization. Both DOS and PDOS indicated that the magnetic moments mainly come from the 2p orbitals of Si atoms and 3p for Mg dopant and 3d orbitals for V dopant. The magnetic moment for 4H-SiC/Mg and 4H-SiC/V was calculated to be 2.23 μB and 3.24 μB.

Keywords: Hexagonal Silicon carbide (4H–SiC); Substitutional Doping; Electronic; Magnetic properties; Quantum ESPRESSO.

I. INTRODUCTION

Silicon carbide (SiC) has been used as an industrial material since the last century, with methods of its synthesis introduced as far back as 1885 [1]. Silicon carbide has been recognized as an important structural ceramic material because of its unique combination of properties, such as excellent oxidation resistance, high wear resistance,

high thermal conductivity and good thermal shock resistance. Such a combination of properties is determined by the highly covalent (up to 88%) chemical bonding between silicon and carbon atoms. However, this very same bonding presents a problem in dense SiC production using powder technology due to the extremely low self-diffusion coefficient, densification of the SiC powders alone is possible only at extremely high pressure and/or temperatures exceeding $2100\ °C$. To densify SiC successfully the use of sintering aids is necessary [2].

Silicon carbide (SiC), also known as carborundum is a semiconductor containing silicon and carbon. It occurs in nature as the extremely rare mineral moissanite. Synthetic SiC powder has been mass-produced since 1893 for use as an abrasive. Grains of silicon carbide can be bonded together by sintering to form very hard ceramics that are widely used in applications requiring high endurance, such as car brakes, car clutches and ceramic plates in bulletproof vests [3].

SiC normally come in different polycrystalline types, of which 3C, 4H, and 6H are the most common ones. Moreover, 4H-SiC is suitable for manufacturing high-power electronic devices because of its large forbidden bandwidth (3.26 eV), good thermal conductivity, and relatively small anisotropy [4-6].

To date, research on the growth of 4H-SiC has achieved great success [7-9]. Doping along Carbon has shown strong and harmful effects on the carrier lifetime of 4H-SiC [10, 11]. Previous studies used electron paramagnetic resonance to show doping along carbon in P-type 4H-SiC annealed at high temperatures and analyzed the influence of external environmental changes on the defects, but some basic electrical properties of V_C^+ defects remain to be characterized [12]. Doping in SiC was theoretically studied by employing pseudo-potential calculations without full ionic relaxations and using only a small supercell [13]. Recent studies have performed accurate pseudo-potential calculations with full ionic relaxations employing a large supercell [14-15]. Nevertheless, the present understanding of doping in SiC remains incomplete.

II. COMPUTATIONAL METHOD

The first-principles calculations were carried out using the Quantum ESPRESSO code [15], which is based on the plane-wave pseudo-potential (PWP) method [16]. We have adopted an exchange-correlation function treated by Generalized Gradient Approximation (GGA) [17] and Perdew–Burke–Ernzerhof (PBE) [18]. We used 4H-SiC hexagonal structure with the experimental lattice $a = 3.041$ Å, $c = 9.952$ Å and space group $P6_{3mmc}$ obtained from the online experimental database [19] as shown in Fig. 1(a). For doping, a model of $2 \times 2 \times 2$ 4H-SiC supercell with 64 atoms was generated using XCrysden software [20] shown in Fig. 1(b), In each case, a single Mg and V atoms were replaced with one Si which is equivalent to 1.56% doping concentration. Both pure and doped systems were optimized using Broyden-Fletcher-Goldfarb-Shanno (BFGS) approximation with $12 \times 12 \times 1$ and $8 \times 8 \times 1$ Monkhorst-Pack k-points [21] within the Brillion zone respectively. In each, both atomic positions and lattice parameters were optimized until the atomic forces and stresses were smaller than $0.01\ eV/$Å and $0.02\ GPa$ respectively. A plane wave energy cutoff of 330 eV and 300 eV are used for the pure and doped systems respectively. The valence electron configurations of Mg-doped 3C-SiC are $3d^8 4s^2$ for V-doped, $3s^2 3p^2$.

III. RESULTS AND DISCUSSION

A. Structural Geometry

Fig. 1 (a) shows our optimized structure. The structure is three-dimensional. There are two equivalent Si sites. In the first Si site, Si(1) is bonded to one C(1) and three equivalent C(2) atoms to form a corner-sharing SiC4 tetrahedral. The Si(1)–C(1) bond length is 1.90 Å. All Si(1)–C(2) bond lengths are 1.90 Å. In the second Si site, Si(2) is bonded to one C(2) and three equivalent C(1) atoms to form a corner-sharing SiC4 tetrahedral. The Si(2)–C(2) bond length is 1.90 Å. All Si(2)–C(1) bond lengths are 1.89 Å. There are two equivalent C sites. In the first C site, C(1) is bonded to one Si(1) and three equivalent Si(2) atoms to form a corner-sharing CSi4 tetrahedral. In the second C site, C(2) is bonded to one Si(2) and three equivalent Si(1) atoms to form a corner-sharing CSi4 tetrahedral.

The $2 \times 2 \times 2$ supercell model of 4H–SiC with 64 atoms was shown in Fig. 1(b). The large supercells used in the calculations allow us to simulate the distribution of various dopants and their possible magnetic configurations. We also fixed the c-axis size of the supercell to 20.26 Å (twice the primitive cell in that direction) and varied the lateral size of the cell in the basal directions. The dopants (Mg and V) are fixed at the x-marked position. The Si atom at the marked position is substituted by the doped Mg and V atoms, with the silicon vacancy is labelled as V_{Mg-Si} and V_{V-Si} respectively. The selected position x is chosen where both the dopants are mono-doped.

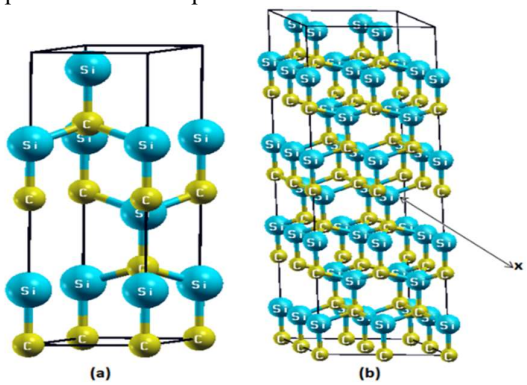

Fig. 1 (a) Optimized Pure 4H SiC (b) $2 \times 2 \times 2$ supercell model with 64 atoms

B. Effect of Doping on Crystal Structure

A single Mg-doped 4H–SiC system was considered first as shown in Fig. 2, with a doping concentration of 1.56%. The hybrid state of Mg and Si after replacing a Si atom with a Mg atom in $2 \times 2 \times 2$ supercells has been calculated. The results show that the maximum magnetic moment is 2.23 μB due to the presence of Mg impurities in the Si site Fig. 2(a). Mg atoms play an important role in the generation of magnetic moments by contributing almost 1.48 μB to the total moment.

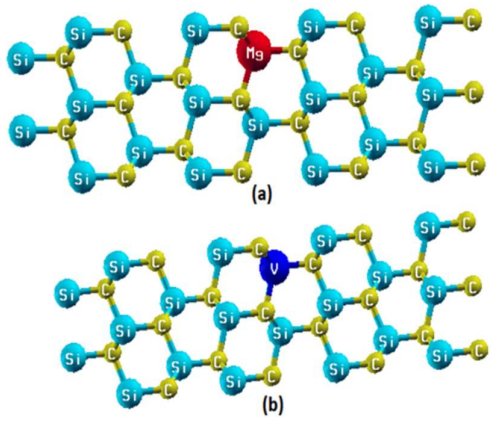

Fig. 2 Substitutional doping model on $2 \times 2 \times 2$ supercell with 64 atoms at chosen reference point x. (a): Single Mg atom doping and (b) Single V atom doping.

Site x was chosen as the research reference point, as shown in Fig. 1(b). The doping concentration of V-doped 4H–SiC is still 1.56%. As a result, the total magnetic moment of the V-doped 4H–SiC system Fig. 2(b) is about 3.24 μB and the V atom plays a major role. Here, a V atom provides a magnetic moment of 2.62 μB. Another important effect is the increase in bond length due to the presence of the impurities dopants, the Si-Mg is found to be 1.89 Å and 2.02 Å for Si-V bond length which are greater than that of Si-C 1.90 Å in pure SiC. These results are in good agreement with the theoretical results in [21-23].

C. Electronic Properties

1) Electronic Band Structure 4H-SiC

Fig. 3 shows our calculated band structure of 4H-SiC crystal with the optimized values, which were also found to be similar to the results reported in [24-25]. From the structure it is clearly shown that the maximum valence band exists at Γ point, while the bottom of the conduction band locates in different k points M, indicating that 4H-SiC is a wide indirect band gap semiconductor with a gap of about 2.22 eV which is less than the experimental value of 3.27 eV [21-25]. The reason the theoretical value is smaller than the experimental value is that the correlation interaction between excited electrons in the calculation model has been underestimated [26] but it is still significant for us to analyze the calculated results.

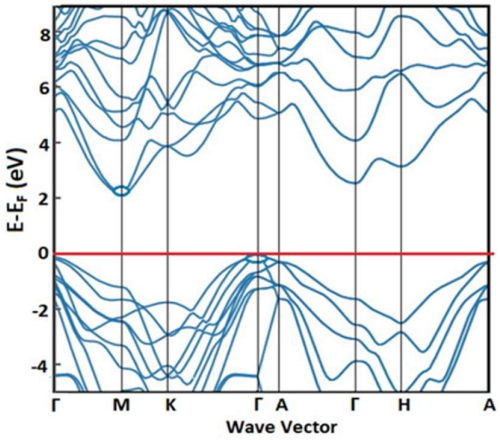

Fig. 3 Calculated Band structure of $2 \times 2 \times 2$ supercell of 4H SiC with DFT-GGA optimized parameters

2) Electronic Band Structure single Mg atom doped 4H-SiC

Fig. 4 shows the calculated band structure of a 2×2×2 supercell with 64-atom doping with a single Mg atom (equivalent to 1.56% doping concentration). The structure indicates a half-metallic behavior with the minority spin being semiconducting along a high symmetry point Γ-A-Γ and the majority spin being metallic with sufficient unfilled states crossing the Fermi level along symmetric point M. These unfilled states behave like free holes, although slightly localized, also it clearly shows an antiferromagnetic (AFM) ordering. This finding indicates that doping 4H SiC with alkaline earth metals changes it from non-magnetic to AFM order. These results are consistent with many theoretical and experimental results for many wide-bandgap materials [31-32].

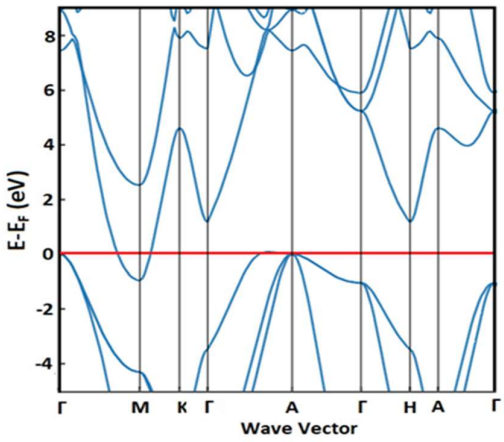

Fig. 4 Calculated Band structure of Mg atom doped $2 \times 2 \times 2$ supercell of 4H SiC with DFT-GGA optimized parameters

3) Electronic Band Structure V doped 4H-SiC

Fig. 5 show the calculated electronic band structure of the Vanadium atom doped 4H SiC. It can be seen that the spin splitting occurs between up spin and down spin channels near the Fermi level, which implies that the V dopants can order magnetism in the $2 \times 2 \times 2$ supercell of SiC. The doped system shows a metallic nature in which the Fermi energy passes through the conduction and valence band in almost all the high symmetry points. This is completely different when V doped 3H cubic SiC as well as other crystal types [26-28], where the authors found that the system of V doped in 3H cubic SiC is half-metallic. Similarly, from our result, it can be seen that the impurity band merges with the conduction band at higher carrier concentrations and the V dopant acts as a donor in SiC. The V dopant is found to be the main contributor to the ferromagnetic (FM) of the V-doped SiC similar case of the Mg-doped system. To have more clear features of what the band structures say, we calculated the spin-polarized DOS and PDOS of the doped systems. Firstly, we modernized our supercell model by considering two by two of $2 \times 2 \times 2$ supercell of 4H SiC supercell. The two models of the Mg and V-doped SiC supercell.

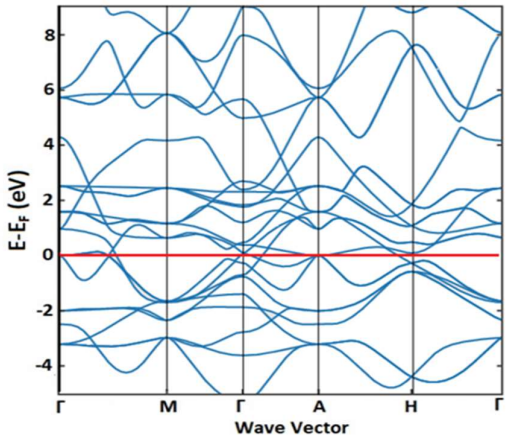

Fig. 5 Calculated Band structure of V atom doped $2 \times 2 \times 2$ supercell of 4H SiC with DFT-GGA optimized parameters

4) DOS and PDOS of Single Mg atom Doped 4H SiC

For our Mg-doped 4H SiC, the calculated DOS and PDOS are presented in Fig. 6 (a) and (b) respectively. From Fig. 6(a), one can see that, due to the Mg impurities, the total DOS indicate that Mg-doped 4H SiC is magnetic in nature with the presence of ferromagnetism (FM) ordered configuration. From Fig. 6(b), the PDOS indicates that the p states of the impurities and host Si atoms overlap significantly in the spin-splitting bands, suggesting a strong hybridization between them. 2pSi–3pV interactions between Mg and neighbouring Si atoms lead to several holes in Mg-doped systems, and therefore the pronounced spin polarization consists mostly of the p orbitals of the nearest neighbour Si atoms around the dopants. Furthermore, the p orbital of Si atoms is rather spatially extended. In comparison to most of the conventional metal dopants, it is expected that the more spatially extended spin-polarized holes in Si 2p states induced by Mg doping, these results show significant similarities with the case of Mg-doped 3H cubic SiC [30].

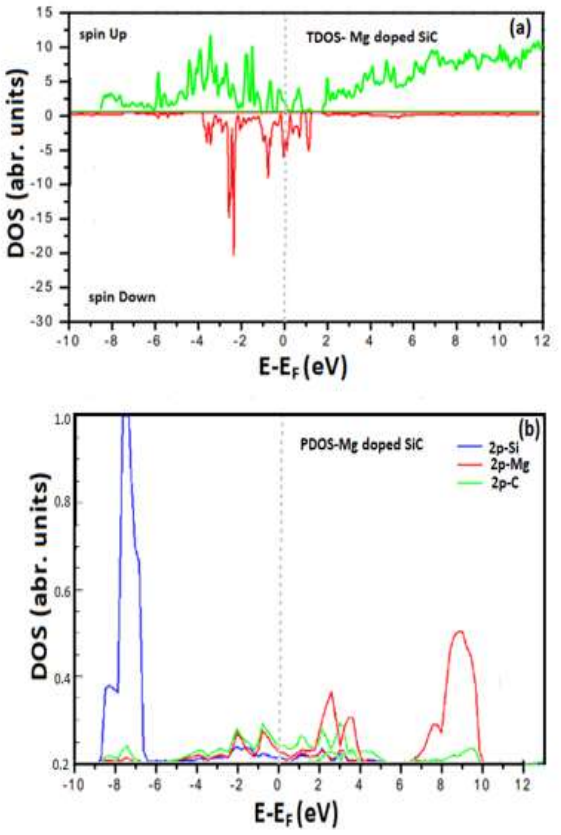

Fig. 6 Calculated (a) Total DOS and (b) PDOS of Mg atom doped 4H SiC

5) DOS and PDOS single V atom doped 4H Si

The calculated TDOS and PDOS for V doped 4H SiC are shown in Fig. 7(a) and (b) respectively. The TDOS in Fig. 7(a) indicate that there is evidence of spin-split around the Fermi level, confirming the possible existence of local magnetic moments as predicted by the electronic band structure. The PDOS plot in Fig. 7(b) shows the presence of V marked difference between the spin-majority (occupied) and the spin-minority (unoccupied) states showing prominent energy splitting at the Fermi level, giving rise to spin polarization. Both Fig. 7(a) and (b) indicate that the magnetic moments mainly come from the 2p orbitals of Si atoms and 3d orbitals of the V dopant. The calculated result also shows that the total magnetic moment is 2.12 μB per supercell.

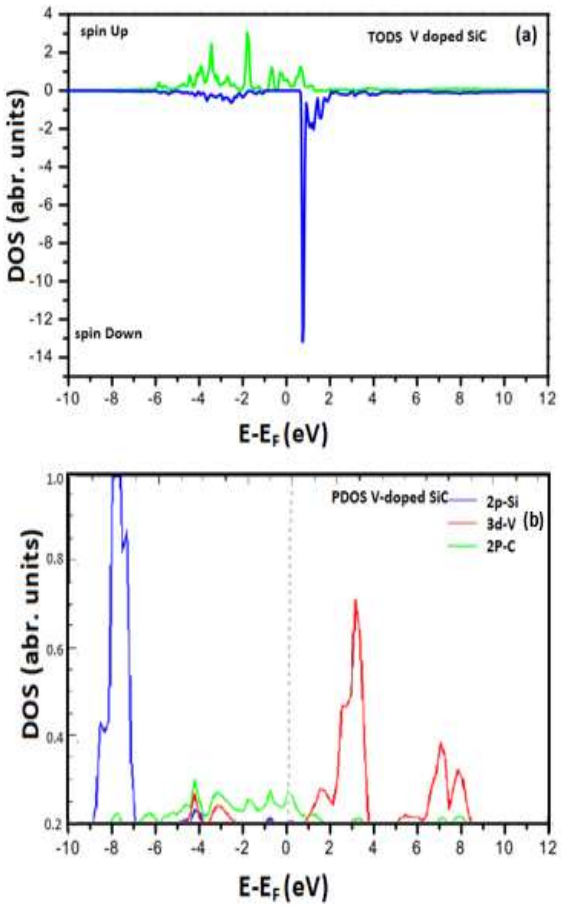

Fig. 7 Calculated (a) Total DOS and (b) PDOS of V atom doped 4H SiC

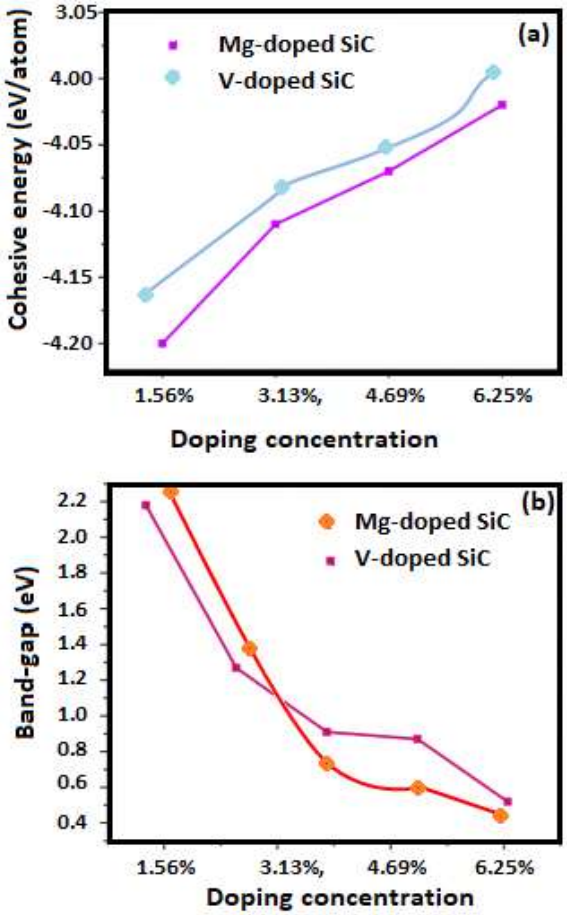

Fig. 8 (a) The graph between doping concentration and cohesive energy (b) The graph between doping concentration and band gap.

D. Magnetic properties

The effect on the cohesive energy and band gap, with the increase in doping concentration, has been investigated. The concentration is increased by increasing the number of substitutional dopants (Mg and V) in $2 \times 2 \times 2$ supercell of 4H SiC, i.e. by substituting 2Mg and V, 3Mg and V and 4Mg and V which is equivalent to 3.125%, 4.6875% and 6.25 %A percentages of doping concentration respectively, From the graph of cohesive energy against doping concentration (see Fig. 8 (a)), we observed a significant increase in a regular manner in both dopants cases, that is as increase the doping concentration the cohesive energy also increases which shows that the structure will become more unstable [33]. Nonetheless, in the case of Band-gap against doping concentration Fig. 8(b) as we increase the doping concentration the band gap is decrease in all the dopants situations. At a point when maximum doping concentration (6.25%) becomes consistent, however variety in doping concentration sites a significant change happens in the band gap of all the doped systems.

IV. CONCLUSION

In conclusion, we have systematically investigated the effect of Mg and V atoms doping 4H–SiC within the framework of DFT-GGA as implemented in Quantum ESPRESSO. The following deductions have been drawn:

1. The presence of both alkaline earth metal and transition metal into a non-magnetic 4H–SiC compound can significantly transform it into a magnetic material with a significant magnetic moment.
2. The electronic band structure of pure 4H-SiC is a wide indirect band gap semiconductor with a gap of about 2.21 eV which is less than the experimental value of 3.27 eV [34], and also observed a half-metallic behavior with the minority spin being semiconducting along a high symmetry point Γ-A-Γ and the majority spin being metallic with sufficient unfilled states crossing the Fermi level along symmetric point M.
3. Introducing Mg and V impurities completely shrinks the band gap and turns the material into a metallic

nature, also making a Fermi energy pass through the conduction and valence band in almost all the high symmetry points. The V dopant is found to be the main contributor to the ferromagnetic (FM) of the V-doped SiC similar case of the Mg-doped system. These results show that the doped systems can be a favorable candidate in Spintronic applications.

4. Finally, by varying the doping concentration in increasing paths, the band gap will continue to decrease until a maximum concentration is achieved where the band gap shrinks completely while the cohesive energy is also increased.

References

[1] V. A. Izhevskyi, L. A Genova, J. C. Bressiani, and A. H. A. Bressiani, “Silicon carbide. Structure, properties and processing”. *Cerâmica*, vol. *46, no.* 297, pp. 4-13, 2000.

[2] D. L. Zhao, F. Luo and W. C Zhou, “Microwave absorbing property and complex permittivity of Nano SiC particles doped with nitrogen”, *J. of Alloys & Comp.*, vol. 490, pp. 190–194, 2010.

[3] D. Zhao, Z. Hongshen and Z. Wanchen, "Dielectric properties of nano Si/C/N composite powder and nano SiC powder at high frequencies." *Physica E: Low-dimensional Sys. & Nanostruct, vol.* 9, no. 4, pp. 679-685, 2001.

[4] B. Wenzien, K. Peter, B. Friedhelm, and C. Giancarlo, "Quasiparticle band structure of silicon carbide polytypes." Phy. Rev. B, vol. 52, no. 15 pp. 10897, 1995

[5] R. Fabrizio, P. Fiorenza, G. Greco, R. Lo Nigro, F. Giannazzo, A. Patti and M. Saggio, "Challenges for energy efficient wide band gap semiconductor power devices". Phy, Status Solidi (a), vol. 211, no. 9, pp. 2063-2071, 2014.

[6] V. A. Izhevskyi, L. A Genova, J. C. Bressiani, and A. H. A. Bressiani, "silicon carbide. Structure, properties and processing". Cerâmica, vol. 46, pp. 4-13, 2000.

[7] H. Ta Ching and S. Tsao, "Synthesis and purification of silicon carbide powders for crystal growth." Mat. Sci. Forum, vol. 717, pp. 37-40.

[8] K. Kojima, H. Okumura, S. Kuroda and K. Arai, "Homoepitaxial growth of 4H-SiC on on-axis (0001) C-face substrates by chemical vapor deposition." *J. of Crys. Growth, vol.* 269, no. 2-4 367-376, 2004

[9] I. Akira, T. Tsunenobu Kimoto and H. M. Hiroyuki Matsunami, "Exciton-related photoluminescence in 4H-SiC grown by step-controlled epitaxy." *Jap. J. of App. Phy., vol.* 35, no. 8R, pp. 43-73, 1996.

[10] J. Chao, D. Morgan and I. Szlufarska, "Structures and stabilities of small carbon interstitial clusters in cubic silicon carbide". *Acta materialia*, vol. 62, pp. 162-172, 2014.

[11] Z. M. Ellen, W. W. Lee, H. Yan Wang, W. C. Mitchel, and W. D. Mitchell, "Deep level point defects in semi-insulating SiC". *Mat. Sci, Forum*, vol. 527, pp. 517-522, 2006.

[12] W. Xiuhong, Z. Xu, M. Rommel, B. Dong, Le Song, C. Augustine, T. H Tee, and F. Fang, "Electron paramagnetic resonance characterization of aluminium ion implantation-induced defects in 4H-SiC". *Nanotech. & Precision Eng., vol.* 2, no. 4, pp. 157-162, 2019.

[13] C. Wang, J. Bernholc and R. F. Davis, "Formation energies, abundances, and the electronic structure of native defects in cubic SiC". *Phy. Rev. B, vol.* 38, no. 17, pp. 12752, 1988.

[14] J. Lento, M. Pesola, J.-L. Mozos and R. M. Nieminen, "Vacancies in SiGe: Jahn–Teller distortion and spin effects". App. Phy. Lett. vol. 77, no. 2, pp. 232-234, 2000.

[15] G. Paolo, S. Baroni, N. Bonini, M. Calandra, R. Car, C. Cavazzoni and D. Ceresoli "QUANTUM ESPRESSO: a modular and open-source software project for quantum simulations of materials." *J. of Phy: Cond. Matt., vol.* 21, no. 39, pp. 395502, 2009

[16] T. Norman and J. Luís Martins. "Efficient pseudo potentials for plane-wave calculations." *Phy. Rev. B,* vol. 43, no. 3, pp. 19-91, 1993.

[17] B. Kieron, J. P. Perdew and M. Ernzerhof, "Why the generalized gradient approximation works and how to go beyond it". *Inter. J. of Quantum Chem., vol.* 61, no. 2, pp. 287-293, 1997.

[18] E. Matthias and G. E. Scuseria, "Assessment of the Perdew–Burke–Ernzerhof exchange-correlation functional". *The J. of Chem. Phy., vol.* 110, no. 11, pp. 5029-5036, 1999.

[19] J. Anubhav, S. Ping Ong, G. Hautier, W. Chen, W. Davidson Richards, S. Dacek and S. Cholia, "Commentary: The Materials Project: A materials genome approach to accelerating materials innovation". *APL Mat., vol.* 1, no. 1, pp. 01-12, 2013.

[20] A. Kokalj, "XCrySDen—a new program for displaying crystalline structures and electron densities". *J. of Mole. Graphics and Model, vol.* 17, no. 3-4, pp. 176-179, 1999.

[21] H. J. Monkhorst and J. D. Pack, "Special points for Brillouin-zone integrations". *Phy. Rev. B, vol.* 13, no. 12, pp. 5188, 1976.

[22] Y. Lin, H. Jin, D. Liu, Y. Dai, M. Guo, B. Huang, and Z. Zhang, "Investigation of ferromagnetism in Al-doped 4H–SiC by density functional theory". *Chem. Phy. Lett, vol.* 496, no. 4-6, pp. 276-279, 2010.

[23] L. Long, J. Huang, W. Yu, H. Tao, L. Zhu and P. Wang, "Electronic structures and magnetic properties of Co-, Mn-doped and (Co, Mn) co-doped 4H–SiC: A first-principles study". *Vacuum, vol.* 172, pp. 109091, 2020.

[24] D. Yankun, H. Jin, M. Cao, X. Fang, Z. Hou, Dan Li and S. Agathopoulos, "Structural stability, electronic and optical properties of Ni-doped 3C–SiC by first principles calculation". *J. of Alloys and Comp., vol.* 509, no. 20, pp. 6117-6122, 2011.

[25] Z. Bing, L. Zhu, L. Lin, W. Yu, H. Tao, Y. Xu, F. Guo, L. Li and J. Huang. "Electronic structures and ferromagnetism in (Fe, Cr) codoped 4H–SiC from first principles investigations." *Vacuum, vol.* 167, pp. 59-63, 2019.

[26] D. Andreas and M. Head-Gordon, "Single-reference ab initio methods for the calculation of excited states of large molecules". *Chem. Rev., vol.* 105, no. 11, pp. 4009-4037, 2005.

[27] C. Hun Jae, "Effect of doping on properties of hexagonal polytype silicon carbide crystals." Ph.D. dissertation, Carnegie Mellon Univ., 2005.

[28] P. J. Anthony, "*Growth of 2H Silicon Carbide Crystals"*. Nat. Aero. & Space Admin., vol. 40, no. 11, pp. 4660-4662. 1969.

[29] U. Yoshitaka, K. Yagi and H. Nagasawa, "Ab initio density functional theory calculation of stacking fault energy and stress in 3C-SiC". *Physica Status Solidi (b), vol.* 249, no. 6, pp. 1229-1234, 2012.

[30] B. H. Morkoc, S. Strite, G. B. Gao, M. E. Lin, B. Sverdlov, and M. Burns, "Large-band-gap SiC, III-V nitride, and II-VI ZnSe-based semiconductor device technologies". *J. of App. Phy.,* vol. 76, no. 3, pp. 1363-1398, 1994.

[31] W. Geming, H. Lin, C. Lin, S. Liu, Shenggao Wang and Q. Deng, "Effects of alkaline-earth dopants on structural, optical and magnetic properties of $Bi_2Fe_4O_9$ powders". *J. of Mat. Sci: Mat. in Elect. vol.* 28, no. 21, pp. 15797-15803, 2017.

[32] W. Adli and A. H. Belbachir, "A first principles investigation of electronic structure and ferromagnetic properties in alkali metal-doped ZnS/Se semiconductors". *J. of Comp. Elect., vol.* 21, no. 5, pp. 1061-1069, 2022.

[33] B. Giovanna, B. Talamini, A. Renuka Balakrishna, Y. Chiang and W. Craig Carter, "Mechanical instability of electrode-electrolyte interfaces in solid-state batteries". *Phy. Rev. Mat., vol.* 2, no. 10, pp. 105-107, 2018.

[34] T. Guannan, X. Tang, Y. Zhang, Y. Zhang and Q. Song, "Study of the SiO 2/4H-SiC Interface Obtained by Oxidation of Nitrogen Doped Nanoscale Epitaxial Layer". In *2018 1st Workshop on Wide Bandgap Power Devices and Applications in Asia (WiPDA Asia)*, IEEE, pp. 233-238, 2018.